# Insight into In Situ Amphiphilic Functionalization of Few-Layered Transition Metal Dichalcogenide Nanosheets

*Jianfeng Shen, Jingjie Wu, Man Wang, Yuancai Ge, Pei Dong, Robert Baines, Gustavo Brunetto, Leonardo D. Machado, Pulickel M. Ajayan,* and Mingxin Ye**

Layered transition-metal dichalchogenides (LTMDs) have recently attracted critical attention due to their potential applications in optoelectronics, catalysis, and composite synthesis.[1–3] However, LTMDs sheets tend to irreversibly subside in solutions since they restack within a short period of time.[4,5] LTMD-based materials need to be sufficiently dispersible in different solvents.[6] Thus, the ability to exfoliate and chemically modify the surface of LTMDs sheets is an imperative for practical applications such as nanocomposite synthesis and energy storage.

Recently, the functionalization of LTMDs[7,8] to improve their dispersibility through covalent and non-covalent routes has been a research hot spot.[5,9] Furthermore, functionalization of LTMDs with different kinds of polymers is of particular interest, which can greatly enhance the compatibility of the functionalized LTMDs in polymer matrix.[10] As to the functionalization and dispersion of LTMDs with polymers, from the scientific point of view, three issues are of great concern: (i) how are surface conditions affected by polymers?; (ii) what are the main factors underlying the process of stabilization?; (iii) can the dispersibility and stability of the functionalized LTMDs nanosheets be controlled? So far, on the one hand, different functionalized LTMDs nanosheets can only be dispersed in certain solvents, while amphiphilic ones that can be dispersed in both water-miscible solvents with high polarity (such as water and methanol) and organic solvents with low polarity (such as xylene and hexane) have rarely been explored. On the other hand, the interactions between polymers and LTMDs in the functionalization process are scarcely discussed.

Therefore, although significant progress toward functionalization of LTMDs has been made, precisely tuning and studying their surface properties is still a great challenge.[2,11] Herein, for the first time, we demonstrate a solution to the issue of amphiphilic LTMDs by systematically studying copolymer functionalization of LTMD nanosheets. Our basic strategy entails complete exfoliation of LTMDs followed by in situ polymerization of copolymers. Interestingly, the copolymer-functionalized LTMDs nanosheets boost the dispersibility in solvents with different polarities. In addition, the dispersibility of the functionalized LTMD can be further tuned by adjusting the two segments on the copolymers. Surface tension components, polarity and coordination effects of the copolymer are found to be the main factors affecting the dispersibility of the functionalized LTMDs in different solvents. The effect of improved dispersibility is clearly demonstrated in the enhanced mechanical and thermal behaviors of the composites. Furthermore, it is intriguing that this functionalization method is universal to be applied to other LTMDs, such as $MoSe_2$, $WS_2$, and $WSe_2$. As a result, this method is promising for processing LTMDs nanosheets in different solvents and composites, an application area where LTMDs nanosheets are expected to play an important role in the near future.

While electronic and optical devices require the design of suitable patterns to govern their properties, the principle motivating factor for the functionalization of LTMDs is the integration and compatibility of solvents and condensed-phase systems. In this work, we use $MoS_2$ nanosheets as the model for functionalization since it is the most studied instance of a quasi-2D LTMD. It has been concluded that bulk $MoS_2$ consists of 2D layers held together by weak van der Waals forces and proper solvents enable the successful exfoliation of $MoS_2$. In current work, a non-toxic mixture of 2-propanol (IPA)/water (7:3 by volume) was used for the liquid phase exfoliation (LPE) of bulk $MoS_2$ powder. It exhibited similar exfoliation efficiency as conventional N-methyl-2-pyrrolidone,[7,12] while its low boiling point further facilitated functionalization. Covalent functionalization of LTMDs has been relatively limited on account of LTMDs' strong chemical stability within reactive organic and aqueous systems. Consequently, researchers have pursued highly reactive radical-based functionalization strategies to impart specific properties to LTMDs. Following suit,[13] after LPE of $MoS_2$, several polystyrene (PS)–polyacrylamide (PAM) grafted copolymers were synthesized simultaneously on exfoliated $MoS_2$ nanosheets by in situ living free-radical polymerization (**Figure 1**a). Details on the synthesis are provided in the Experimental Section of the Supporting Information, Section S1, while the formulation for the synthesis of PS-PAM-LTMDs nanocomposites can be found in Table S1 of the Supporting Information. The dispersibility of PS-PAM copolymer functionalized $MoS_2$ nanocomposites (PS-PAM-$MoS_2$) was tested in a number of solvents, including hexane, carbon tetrachloride ($CCl_4$), xylene, n-butyl alcohol (NBA), tetrahydrofuran (THF), IPA, chloroform ($CHCl_3$), acetone, acetonitrile (ACN),

Prof. J. Shen, M. Wang, Y. Ge, Prof. M. Ye
Institute of Special Materials and Technology
Fudan University
Shanghai 200433, P. R. China
E-mail: mxye@fudan.edu.cn
Prof. J. Shen, Dr. J. Wu, Dr. P. Dong, R. Baines, G. Brunetto, Dr. L. D. Machado, Prof. P. M. Ajayan
Department of Materials Science and NanoEngineering
Rice University
6100 Main Street, Houston, TX 77005, USA
E-mail: ajayan@rice.edu
Dr. G. Brunetto, L. D. Machado
Department of Applied Physics
State University of Campinas
Campinas, SP 13083-959, Brazil

**DOI: 10.1002/adma.201602887**

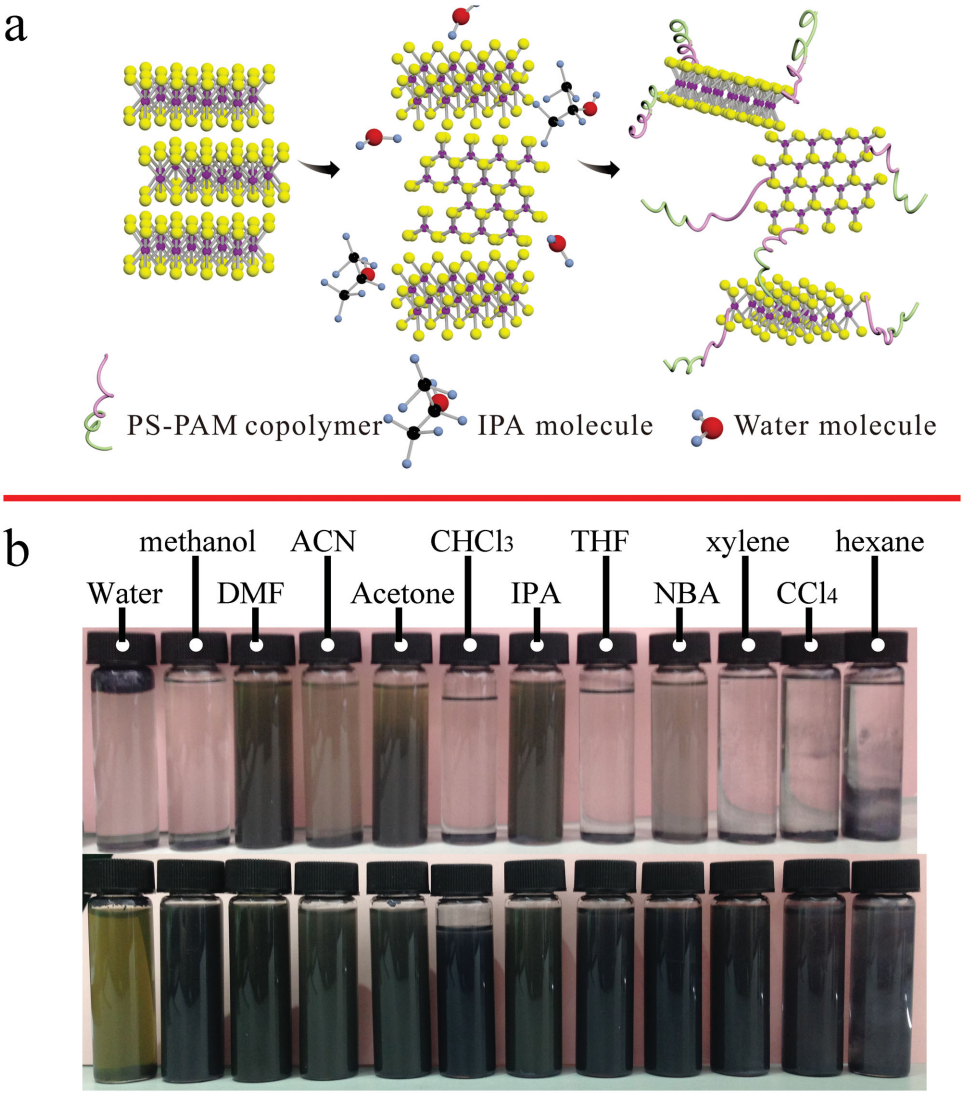


**Figure 1.** a) Process for preparation of PS-PAM-LTMDs nanocomposites; b) Photographs of pristine $MoS_2$ (upper row) and PS-PAM-$MoS_2$ (lower row) dispersed in different solvents.

dimethyl formamide (DMF), methanol, and water. Compared to pristine $MoS_2$, PS-PAM-$MoS_2$ disperses well in these solvents and yields homogeneous solutions (Figure 1b). These solutions can last for weeks, indicating the excellent stability of PS-PAM-$MoS_2$.

To further demonstrate the efficacy of our method, the dispersibilities of PS-PAM-$MoS_2$ with different copolymer weight percentages are presented in **Figure 2**. Generally, compared to pristine $MoS_2$, all the PS-PAM-$MoS_2$ nanocomposites dispersed much better in solvents with different polarity (1-2 orders of magnitude higher). When the weight ratio of PS to $MoS_2$ was fixed, a higher amount of PAM facilitated dispersion of the nanocomposites in high polar solvents like water, while a higher amount of PS promoted dispersibility in solvents with lower polarity such as hexane and DMF (Figure 2a). In another case, when the weight ratio of PS to PAM was fixed, nanocomposites with different amounts of $MoS_2$ also demonstrated dissimilar dispersibilities (Figure 2b), which implies that the contents of the PS-PAM copolymer heavily influenced the dispersibility of the nanocomposites. Typical UV–vis spectra of $PS_{20}$-$PAM_{10}$-$MoS_2$ nanosheets suspended in different solvents (water, DMF, and hexane) are shown in Figure S1 of the Supporting Information. The $PS_{20}$-$PAM_{10}$-$MoS_2$ nanosheets suspensions feature two distinct peaks around 629 and 675 nm, which can be attributed to characteristic direct excitonic transitions ($A_1$ and $B_1$) with the energy split from valence band spin-orbital coupling.[12] We attribute the enriched dispersibility of the nanocomposites to the wrapping of in situ polymerized PS-PAM on $MoS_2$ nanosheets after the propagation and adsorption of PS-based macro radicals, which reduces van der Waals interactions and promotes the isolation of $MoS_2$ sheets in solution. Consequently, in accordance with the rule of "like dissolves like", the PS component boosts the dispersibility of PS-PAM-$MoS_2$ in solvents with low

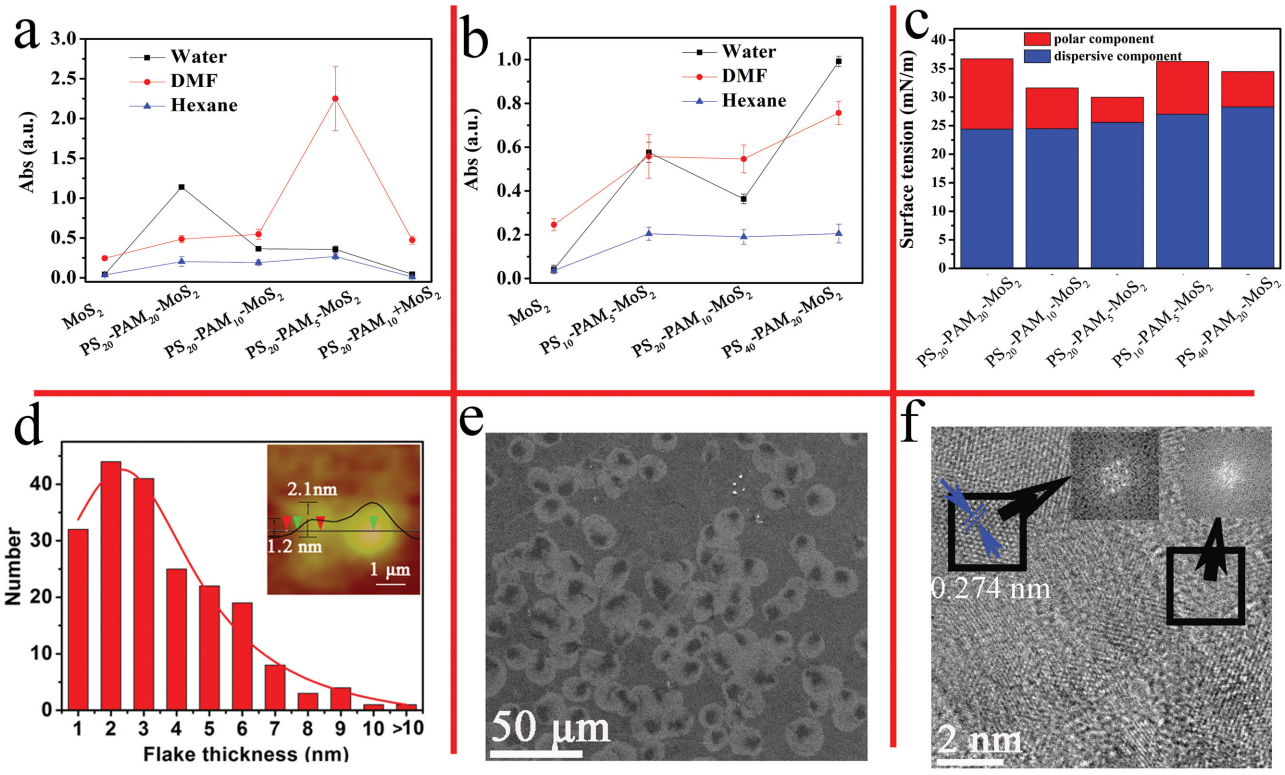


**Figure 2.** Dispersibility of PS-PAM-$MoS_2$ nanocomposites at 629 nm with different ratios of PS, PAM, and $MoS_2$. a) The ratio of PS to $MoS_2$ was fixed; b) the ratio of PS to PAM was fixed) in different kinds of solvents of hexane (low polarity), DMF (medium polarity), and water (high polarity). c) Surface tension components of different PS-PAM-$MoS_2$ nanocomposites. Histogram of the numbers of various flake thicknesses of $PS_{20}$-$PAM_{10}$-$MoS_2$ obtained by d) AFM and e) SEM. f) High-resolution TEM analysis of typical exfoliated $PS_{20}$-$PAM_{10}$-$MoS_2$ nanosheets. The arrows depict the position of the $MoS_2$ and assembled PS-PAM (insets are the reduced FFT patterns of the corresponding HRTEM images).

polarity, while the hydrophilic PAM part enhances dispersion in high polar ones.[8,14]

It is known that the functionalization of LTMDs is critical for tailoring their surface properties to specific solvents and environments.[7] To gain deeper insight into factors influencing the nanocomposites' dispersibility, the surface tension components of the PS-PAM-$MoS_2$ nanosheets were characterized and analyzed side by side (Figure 2c). Clearly, as PAM segment ratios increase, polar component accentuates. On the other hand, as the PS segment ratios increase, the dispersive component is boosted. Both trends are consistent with the dispersibility of the nanocomposites in solvents with different polarities.

X-ray diffraction (XRD) analysis of the $MoS_2$-based materials was performed to validate the LPE and functionalization processes. Compared to pristine $MoS_2$, it can be clearly seen that the intensities of the main peaks of PS-PAM-$MoS_2$ nanocomposites decreased by more than two orders of magnitude (Figure S2, Supporting Information). Such indicates that during LPE treatment, the $MoS_2$ crystals reduced in size and the crystallinity was further decreased with the in situ polymerization process. In addition, obvious broadening of the peaks in the diffraction patterns was also observed, which suggests the existence of crystallites in varying nanoscale dimensions during functionalization.[15]

Thermogravimetric analysis (TGA) analysis was used to characterize the thermal properties of the functionalized $MoS_2$ nanosheets. Figure S3 of the Supporting Information illustrates the TGA curves of raw $MoS_2$, PS-PAM, and PS-PAM-$MoS_2$ nanocomposites, while Table S2 of the Supporting Information displays the $T_{max}$ (temperature for the maximum decomposition) of the two peaks and residues of the samples. The obvious difference between the thermal stability of raw $MoS_2$ and PS-PAM helps us determine the content of the copolymer in PS-PAM-$MoS_2$ nanocomposites. It can be found that raw $MoS_2$ is thermally stable in argon atmosphere. In sharp contrast, PS-T and PS-PAM demonstrate 100% weight loss at 500 °C, far below the initial decomposition temperature of raw $MoS_2$. The contents of PS-PAM grafted on $MoS_2$ nanosheets determined by TGA are between 16 and 56 wt%. Furthermore, the PS-PAM-$MoS_2$ nanocomposites demonstrate significantly different weight loss curves and thermally degrade in two stages between 150–350 °C and 350–500 °C. We attribute the first stage to the decomposition of PAM chains and the second stage to the pyrolysis of PS chains.[16] Compared to PS-PAM, the decomposition temperatures of PS-PAM-$MoS_2$ nanocomposites are much higher than those of PS-PAM, which is mainly a result of the barrier effect provided by the exfoliated $MoS_2$ in the nanocomposites.

To study the thickness and morphology of functionalized LTMDs, more than 200 nanosheets of exfoliated $PS_{20}$-$PAM_{10}$-$MoS_2$

were randomly selected and analyzed by atomic force microscopy (AFM). A distribution of the thickness was obtained. As shown in Figure S4a of the Supporting Information, the exfoliated $MoS_2$ nanosheets are separated from each other, suggesting high dispersibility. Compared to a typical thickness for pristine exfoliated $MoS_2$ of about 1.1 nm, the Gauss fitting thickness of $PS_{20}$-$PAM_{10}$-$MoS_2$ is substantially higher (Figure 2d) due to the assembled and coated PS-PAM chains on the surfaces of $MoS_2$ sheets. Scanning electron microscope (SEM) image of the exfoliated $MoS_2$ shows submicrometer-sized nanosheets are finely distributed over the silicon wafer substrate (Figure S4b, Supporting Information). After functionalization with PS-PAM, the coatings on the surface of exfoliated $MoS_2$ can be clearly seen (Figure 2e).

Transmission electron microscopy (TEM) was employed to further analyze the morphology of the samples. As indicated by the obscure image-which would be otherwise clear for highly crystalline $MoS_2$ at the same magnification (Figure S4c, Supporting Information)-the surface of $PS_{20}$-$PAM_{10}$-$MoS_2$ was coated with an amorphous layer (Figure 2f). In fact, only part of the smooth edge of $MoS_2$ sheet is visible (lattice spacing of 0.274 nm is corresponding to (100) plane of $MoS_2$),[17] while the rest is coated with the amorphous layer. The high-resolution TEM (HRTEM) image indicates that some parts of $MoS_2$ are embedded in the PS-PAM layers, which is a factor of the random assembling and coating of PS-PAM on exfoliated $MoS_2$. This finding is also consistent with SEM and AFM images.[3] Fast Fourier transform (FFT) patterns of the different components (indicated by black arrows) clearly demonstrate disparities (exfoliated $MoS_2$ as series of highly ordered diffraction spots, while the amorphous PS-PAM copolymer appears as dispersive circles), and feature the PS-PAM copolymer coating $MoS_2$ crystals. In addition, the connection between the PS-PAM-$MoS_2$ nanocomposites can also be detected (Figures S5–S7, Supporting Information).

Since chalcogen atoms in the basal plane of LTMDs nanosheets are saturated and fairly unreactive, they tend to remain inert during chemical functionalization. Knowing this, we attempted to functionalize $MoS_2$ via in situ polymerization. Fourier transform infrared spectroscopy (FTIR) was used to obtain information regarding the nature of chemical bonds at the surface modification (**Figure 3**a). $MoS_2$ shows its typical peak at 1096 $cm^{-1}$. The finger trace related to PS is observed at 1450 $cm^{-1}$ with stretching of benzene, while the weak peak around 3400 $cm^{-1}$ is from the N–H stretching mode in PAM.[18] A typical amide group constituent has three characteristic peaks: the first is at 1660 $cm^{-1}$ (Amide I), representing the C=O stretching vibration of the amide group. The second peak resides around 1610 $cm^{-1}$ (Amide II), which is primarily due to the $-NH_2$ bending vibration of the amide group. The third one is the −CN stretching vibration of the amide group at 1425 $cm^{-1}$.[18] Evidently, the ratio of the intensities of the above three characteristic peaks remained unchanged as compared to the initial styrene and acrylamide monomers. However, the characteristic peaks of PAM (Figure 3b) and $MoS_2$ (Figure 3c) change with different amounts of PS-PAM. In particular, the peak of N−H undergoes red-shift, which is indicative of the metal ligand and $-NH_2$ bonding.[19,20]

To confirm the successful surface modification of the samples from a chemical component standpoint, X-ray photoelectron spectroscopy (XPS) was conducted. From the entire spectrum of $PS_{20}$-$PAM_{10}$-$MoS_2$ (Figure S8, Supporting Information), five elements, namely, C, O, N, Mo, and S exist. The N 1s spectrum of PS-PAM was deconvoluted into two peaks with binding energies at 399.2 and 401.5 eV, corresponding to $NH_2$ and N (the hydrogen bonding effect in pure PS-PAM is the dominate intermolecular force), respectively.[21] For the N 1s of $PS_{20}$-$PAM_{10}$-$MoS_2$, the peak at 399.2 eV still exists but the peak corresponding to intermolecular force resides at a lower energy (401.0 eV), suggesting that other forces between PS-PAM and $MoS_2$ exist (Figure 3d).[20] Two peaks at 232.7 and 229.5 eV, for Mo $3d_{3/2}$ and $3d_{5/2}$, respectively, can be observed in liquid exfoliated $MoS_2$, verifying the dominant 2H phase in LPE $MoS_2$.[22] However, these peaks are slightly shifted in $PS_{20}$-$PAM_{10}$-$MoS_2$ (Figure 3e). In addition, two other peaks emerged, one at 233.6 and the other at 230.4 eV, testifying to the effect between PS-PAM and $MoS_2$ (mainly the coordination effect between metal and organic groups).[17] Moreover, both the $E^1{}_{2g}$ and $A_{1g}$ modes of $PS_{20}$-$PAM_{10}$-$MoS_2$ were red shifted compared to the Raman spectrum of pristine $MoS_2$, which connotes a possible reaction between PS-PAM and $MoS_2$ (Figure S9, Supporting Information). Therefore, in accordance with the references[7,20,21] and considering FTIR, XPS, and Raman results, a distinct coordination effect between $NH_2$ and Mo leads to the functionalization of PS-PAM-$MoS_2$. Moreover, the dispersions of the functionalized $MoS_2$ nanosheets in different solvents are quite stable (Figure S10, Supporting Information), which further enhances their potential application in different fields.

Fully atomistic molecular dynamics simulations were carried out to better understand the role of PS-PAM copolymer on $MoS_2$ layers. Figure 3f demonstrates the interaction energy between $MoS_2$ layers as a function of the number of polymer chains inserted between them. As expected, the separation between layers increases as the number of chains increases, and this leads to smaller attraction between the $MoS_2$ sheets. As a result, the energy needed to separate the sheets decreases. This correlates well with the observation that, for a fixed PS-PAM ratio, dispersibility increases when the copolymer concentration levels are elevated (Figure 1b). Interestingly, rather nonlinear jumps in the interlayer energy were observed as the concentration increased. The effect of PS-PAM copolymer on the sliding of the sheets was further studied with steered molecular dynamics and the potential of mean force. From Figure 3f, it can be seen that the introduction of copolymer causes an increase in the necessary energy to slide the sheets. For a copolymer concentration of 14.4 wt%, we observe two possibilities for the initial configurations. However, when the copolymer concentration is decreased to 7.7 wt%, no bound in all the edges was observed since the $MoS_2$ sheets did not change their curvature enough to allow the bound edges with the low concentration of copolymer. The highest energy necessary to displace the sheets was found at a copolymer concentration of 14.4 wt% and when the sheet edges were bounded. This behavior can be explained by considering how an applied external force needs to bend the sheets and displace the copolymer, which is wrapped by the sheets. The second highest energy to displace the sheet occurs when the polymer concentration is 7.7 wt%. For that particular concentration, we

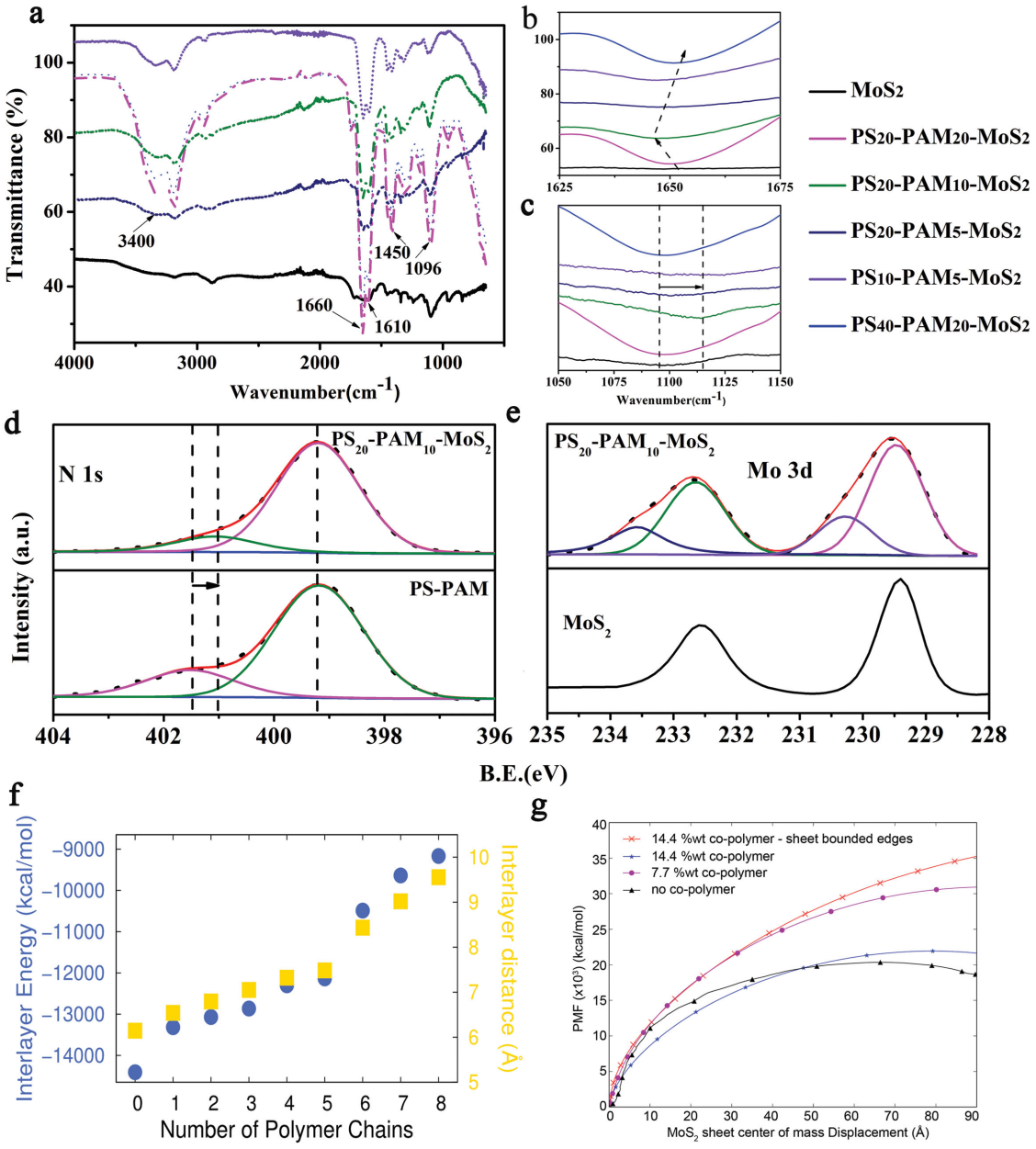


**Figure 3.** a–c) FTIR spectra of PS-PAM and PS-PAM-$MoS_2$ nanocomposites; d) high XPS resolution N 1s of PS-PAM and $PS_{20}$-$PAM_{10}$-$MoS_2$; e) Mo 3d of $MoS_2$ and $PS_{20}$-$PAM_{10}$-$MoS_2$; f) Interlayer energy (blue circles) and interlayer distance (yellow squares) for two $MoS_2$ sheets as a function of the number of polymer chains inserted between them; g) potential of mean force calculated for the four possibilities considered.

observed that the sheets were in contact in some regions but during the pulling procedure the sheets needed to change their shapes and also displace the copolymer (see Figure 3g, Movie S1, Figure S11, and detailed discussion in Section 3 of the Supporting Information).

As a typical layered inorganic material, if $MoS_2$ nanosheet could be perfectly exfoliated and dispersed in polymers, the resulting physical barrier would inhibit the diffusion of heat, facilitate load transfer in the matrix, and effectively ameliorate their thermal stabilities and mechanical properties. PS, which can be dissolved in xylene, a solvent with low polarity, was selected as the polymer matrix to study the effect of PS-PAM-$MoS_2$ composites on their thermal and mechanical properties. Figure S12a,b of the Supporting Information shows the thermal stabilities of PS-based composites with different kinds and amounts of nanofillers. It can be observed that $T_{max}$ and $T_{10\%}$ (temperature for 10% decomposition) of all the composites are much higher than those of pure PS. After adding 1 wt% $PS_{20}$-$PAM_{10}$-$MoS_2$, $T_{max}$ and $T_{10\%}$ of the composites increased to 436 and 425 °C, which are 24 and 31 °C higher than those of pure PS, respectively. This indicates that the presence of exfoliated PS-PAM-$MoS_2$ can effectively defer the thermal

degradation of PS.[4] In order to ascertain mechanical robustness, a tensile test was conducted using a microtensile tester with a 200 N load cell. As shown in Figure S12c,d of the Supporting Information, the tensile strength and tensile modulus of the PS matrices tend to increase in tandem with the addition of PS-PAM-$MoS_2$. Since PS-PAM-$MoS_2$ has excellent compatibility with xylene, the solvent used for film preparation, and with the PS matrix, fracture energy can be increased and crack propagation can be abated by bringing up the crack faces of PS-PAM-$MoS_2$. Among all tested nanofillers, $PS_{20}$-$PAM_{10}$-$MoS_2$ with 1 wt% provided the best reinforcement effect for PS resin, boasting 84.3% and 97.2% improvement of tensile strength and modulus, respectively. The notable improvement can be attributed to the functional groups on PS-PAM-$MoS_2$, which affect compatibility in the PS matrix. When the amount of PS-PAM-$MoS_2$ increases beyond 4 wt%, its dispersibility across the matrix is undermined and consequently thermal and mechanical performances attenuate (Table S3, Supporting Information). Because of its high surface energy, large aspect ratio, and elevated viscosity, it becomes more difficult for the PS-PAM-$MoS_2$ to disperse in the resin when intensifying its concentration, resulting in less energy dissipating in the system. High-resolution SEM images of the fractured surfaces of the sample after a tensile test (as shown in Figure S12e, Supporting Information) were used to investigate the dispersion and compatibility of PS-PAM-$MoS_2$ in a PS matrix. It can be clearly observed that the fractured surface forms a homogeneous network with the proper amount of PS-PAM-$MoS_2$. A similar morphology is observed as the cryogenically fractured surface (Figure S12f, Supporting Information), displaying the unidirectional stripes of bearing load. In addition, the cross-sectional morphologies of pure PS are riddled with random fracture lines (Figure S13a,b, Supporting Information), while agglomeration of $PS_{20}$-$PAM_{10}$-$MoS_2$ was observed on the surface of PS-2-2 film (Figure S13c,d, Supporting Information) after tensile test. Similar results can be found in PEO-based

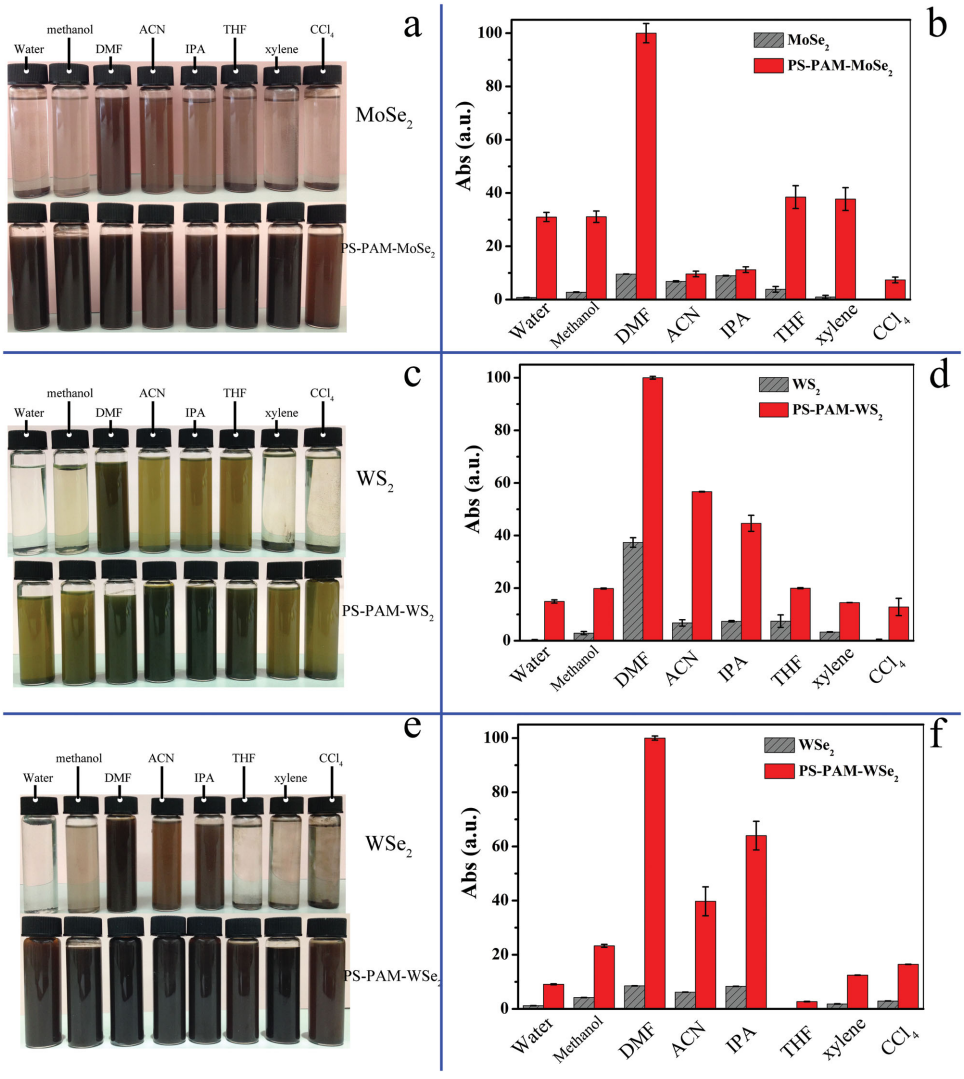


**Figure 4.** a,b) Comparison of photographs and UV–vis results of LTMDs and PS-PAM-LTMDs in different solvents. $MoSe_2$ and PS-PAM-$MoSe_2$; c,d) $WS_2$ and PS-PAM-$WS_2$; e,f) $WSe_2$ and PS-PAM-$WSe_2$.

composites (PEO is a water soluble polymer), which also demonstrated mechanical and thermal properties improvement with little amount of PS-PAM-$MoS_2$ (Figures S14–S16 and Table S4, Supporting Information).

To this end, we have demonstrated that in situ copolymer polymerization is capable of covalently functionalizing $MoS_2$ nanosheets. Actually, this strategy is universal and can be applied to other LTMDs. For example, similar functionalization of exfoliated $MoSe_2$, $WS_2$, and $WSe_2$ nanosheets were achieved. **Figure 4** illustrates how PS-PAM copolymer functionalized LTMDs can be dispersed better in different kinds of solvents compared to pristine LTMDs. Thus, this method to first exfoliate and then second modify the surface of the LTMDs nanosheets in a controlled fashion with amphiphilic copolymer offers viable routes toward technological application such as nanocomposites, catalysis, and energy storage.

In summary, we have prepared PS-PAM-LTMDs nanocomposites with different ratios of PS, PAM, and LTMDs. Apart from the polarity of the copolymer, the coordination effect between the PAM and LTMDs has been demonstrated to be pertinent to the formation of these nanocomposites. Moreover, surface tension components proved to be other important factors governing sufficient functionalization and further dispersion in different solvents. Our method is broadly applicable since it can be achieved by tuning the hydrophilic–hydrophobic balance and the chemical properties of the side chains. The excellent dispersibility of functionalized LTMD-based nanocomposites in different kinds of solvents opens up new opportunities for solution-phase 2D materials processing.

## Supporting Information

Supporting Information is available from the Wiley Online Library or from the author.

## Acknowledgements

This work was financially supported by BRI grant (FA9550-14-1-0268) "Science and Emerging Technology of 2D Atomic Layered Materials and Devices". J.S. acknowledges the financial support from the China Scholarship Council (CSC) and National Natural Science Foundation of China (51202034).

Received: June 1, 2016
Revised: June 25, 2016
Published online: August 4, 2016

[1] a) M. Chhowalla, H. S. Shin, G. Eda, L.-J. Li, K. P. Loh, H. Zhang, *Nat. Chem.* **2013**, *5*, 263; b) Y. Gong, J. Lin, X. Wang, G. Shi, S. Lei, Z. Lin, X. Zou, G. Ye, R. Vajtai, B. I. Yakobson, H. Terrones, M. Terrones, B. K. Tay, J. Lou, S. T. Pantelides, Z. Liu, W. Zhou, P. M. Ajayan, *Nat. Mater.* **2014**, *13*, 1135; c) D. Gopalakrishnan, D. Damien, M. M. Shaijumon, *ACS Nano* **2014**, *8*, 5297; d) H. Li, G. Lu, Y. Wang, Z. Yin, C. Cong, Q. He, L. Wang, F. Ding, T. Yu, H. Zhang, *Small* **2013**, *9*, 1974; e) B. Mahler, V. Hoepfner, K. Liao, G. A. Ozin, *J. Am. Chem. Soc.* **2014**, *136*, 14121; f) S. Najmaei, Z. Liu, W. Zhou, X. Zou, G. Shi, S. Lei, B. I. Yakobson, J.-C. Idrobo, P. M. Ajayan, J. Lou, *Nat. Mater.* **2013**, *12*, 754; g) J. Pan, Z. Wang, Q. Chen, J. Hu, J. Wang, *Nanoscale* **2014**, *6*, 13565; h) D. Voiry, M. Salehi, R. Silva, T. Fujita, M. Chen, T. Asefa, V. B. Shenoy, G. Eda, M. Chhowalla, *Nano Lett.* **2013**, *13*, 6222; i) Q. H. Wang, K. Kalantar-Zadeh, A. Kis, J. N. Coleman, M. S. Strano, *Nat. Nano* **2012**, *7*, 699; j) X. Zhuang, Y. Mai, D. Wu, F. Zhang, X. Feng, *Adv. Mater.* **2015**, *27*, 403.

[2] N. Liu, P. Kim, J. H. Kim, J. H. Ye, S. Kim, C. J. Lee, *ACS Nano* **2014**, *8*, 6902.

[3] W. Liu, X. Yang, Y. Zhang, M. Xu, H. Chen, *RSC Adv.* **2014**, *4*, 32744.

[4] K. Zhou, J. Liu, B. Wang, Q. Zhang, Y. Shi, S. Jiang, Y. Hu, Z. Gui, *Mater. Lett.* **2014**, *126*, 159.

[5] K. Zhou, J. Liu, P. Wen, Y. Hu, Z. Gui, *Appl. Surf. Sci.* **2014**, *316*, 237.

[6] a) A. Castellanos-Gomez, M. Poot, G. A. Steele, H. S. J. van der Zant, N. Agraït, G. Rubio-Bollinger, *Adv. Mater.* **2012**, *24*, 772; b) A. K. Geim, K. S. Novoselov, *Nat. Mater.* **2007**, *6*, 183; c) Z. Tang, Q. Wei, B. Guo, *Chem. Commun.* **2014**, *50*, 3934; d) A. K. Geim, *Science* **2009**, *324*, 1530; e) S. S. Chou, M. De, J. Kim, S. Byun, C. Dykstra, J. Yu, J. Huang, V. P. Dravid, *J. Am. Chem. Soc.* **2013**, *135*, 4584; f) C. Ataca, S. Ciraci, *J. Phys. Chem. C* **2011**, *115*, 13303; g) Q. Tang, D.-E. Jiang, *Chem. Mater.* **2015**, *27*, 3743; h) J. Choi, H. Zhang, H. Du, J. H. Choi, *ACS Appl. Mater. Interfaces* **2016**, *8*, 8864.

[7] C. Backes, N. C. Berner, X. Chen, P. Lafargue, P. LaPlace, M. Freeley, G. S. Duesberg, J. N. Coleman, A. R. McDonald, *Angew. Chem. Int. Ed.* **2015**, *54*, 2638.

[8] X. Qi, K.-Y. Pu, H. Li, X. Zhou, S. Wu, Q.-L. Fan, B. Liu, F. Boey, W. Huang, H. Zhang, *Angew. Chem. Int. Ed.* **2010**, *49*, 9426.

[9] D. Voiry, A. Goswami, R. Kappera, e. SilvaCecilia de Carvalho Castro, D. Kaplan, T. Fujita, M. Chen, T. Asefa, M. Chhowalla, *Nat. Chem.* **2015**, *7*, 45.

[10] a) X. Wang, E. N. Kalali, D.-Y. Wang, *J. Mater. Chem. A* **2015**, *3*, 24112; b) H. Cheng, N. Dong, T. Bai, Y. Song, J. Wang, Y. Qin, B. Zhang, Y. Chen, *Chem. - Eur. J.* **2016**, *22*, 4500; c) Z. Chen, H. Yan, T. Liu, S. Niu, J. Ma, *RSC Adv.* **2015**, *5*, 97883; d) J. Liu, Z. Zeng, X. Cao, G. Lu, L.-H. Wang, Q.-L. Fan, W. Huang, H. Zhang, *Small* **2012**, *8*, 3517; e) Z. Lei, Y. Zhou, P. Wu, *Small* **2016**, *12*, 3112; f) J. Kim, H. Kim, W. J. Kim, *Small* **2016**, *12*, 1184; g) R. C. Selhorst, E. Puodziukynaite, J. A. Dewey, P. Wang, M. D. Barnes, A. Ramasubramaniam, T. Emrick, *Chem. Sci.* **2016**, *7*, 4698.

[11] a) A. Ciesielski, P. Samori, *Chem. Soc. Rev.* **2014**, *43*, 381; b) U. Halim, C. R. Zheng, Y. Chen, Z. Lin, S. Jiang, R. Cheng, Y. Huang, X. Duan, *Nat. Commun.* **2013**, *4*; c) Y. Hernandez, V. Nicolosi, M. Lotya, F. M. Blighe, Z. Sun, S. De, I. T. McGovern, B. Holland, M. Byrne, Y. K. Gun'Ko, J. J. Boland, P. Niraj, G. Duesberg, S. Krishnamurthy, R. Goodhue, J. Hutchison, V. Scardaci, A. C. Ferrari, J. N. Coleman, *Nat. Nano* **2008**, *3*, 563; d) N. I. Kovtyukhova, Y. Wang, A. Berkdemir, R. Cruz-Silva, M. Terrones, V. H. Crespi, T. E. Mallouk, *Nat. Chem.* **2014**, *6*, 957; e) T. Heine, *Acc. Chem. Res.* **2015**, *48*, 65; f) S. Jiang, M. Q. Arguilla, N. D. Cultrara, J. E. Goldberger, *Acc. Chem. Res.* **2015**, *48*, 144; g) M. Naguib, Y. Gogotsi, *Acc. Chem. Res.* **2015**, *48*, 128; h) H. Yuan, H. Wang, Y. Cui, *Acc. Chem. Res.* **2015**, *48*, 81.

[12] G. Cunningham, M. Lotya, C. S. Cucinotta, S. Sanvito, S. D. Bergin, R. Menzel, M. S. P. Shaffer, J. N. Coleman, *ACS Nano* **2012**, *6*, 3468.

[13] J. Shen, Y. He, J. Wu, C. Gao, K. Keyshar, X. Zhang, Y. Yang, M. Ye, R. Vajtai, J. Lou, P. M. Ajayan, *Nano Lett.* **2015**, *15*, 5449.

[14] J. Shen, Y. Hu, C. Li, C. Qin, M. Ye, *Small* **2009**, *5*, 82.

[15] J. Xie, H. Zhang, S. Li, R. Wang, X. Sun, M. Zhou, J. Zhou, X. W. Lou, Y. Xie, *Adv. Mater.* **2013**, *25*, 5807.

[16] Y.-T. Liu, X.-M. Xie, X.-Y. Ye, *Carbon* **2011**, *49*, 3529.
[17] J. Wang, Z. Wu, K. Hu, X. Chen, H. Yin, *J. Alloys Compd.* **2015**, *619*, 38.
[18] L. T. Chiem, L. Huynh, J. Ralston, D. A. Beattie, *J. Colloid Interface Sci.* **2006**, *297*, 54.
[19] R. Lei, X. Jie, X. Jun, Z. Ruiyun, *J. Appl. Polym. Sci.* **1994**, *53*, 325.
[20] K. B. Yatsimirskii, V. V. Nemoskalenko, V. G. Aleshin, Y. I. Bratushko, E. P. Moiseenko, *Chem. Phys. Lett.* **1977**, *52*, 481.
[21] T. Ni, G.-S. Huang, J. Zheng, P. Gao, M.-M. Chen, *Polym. J.* **2010**, *42*, 357.
[22] B. L. Li, L. X. Chen, H. L. Zou, J. L. Lei, H. Q. Luo, N. B. Li, *Nanoscale* **2014**, *6*, 9831.